analytical chemistry

Article

pubs.acs.org/ac

In Situ Analysis of Small Populations of Adherent Mammalian Cells Using Laser Ablation Electrospray Ionization Mass Spectrometry in Transmission Geometry

Rachelle S. Jacobson, Richard L. Thurston, Bindesh Shrestha, and Akos Vertes*

Department of Chemistry, W. M. Keck Institute for Proteomics Technology and Applications, The George Washington University, Washington DC, 20052, United States

Supporting Information

ABSTRACT: Most cultured cells used for biomedical research are cultured adherently, and the requisite detachment prior to biochemical analysis might induce chemical changes. This is especially crucial if accurate metabolic measurements are desired, given the rapid turnover of metabolites in living organisms. There are only a few methods available for the nontargeted in situ analysis of small adherent cell populations. Here we show that laser ablation electrospray ionization (LAESI) mass spectrometry (MS) can be used to analyze adherent cells directly, while still attached to the culture surface. To reduce the size of the analyzed cell population, the spot size constraints of conventional focusing in reflection geometry (rg) LAESI had to be eliminated. By introducing transmission geometry (tg) LAESI and incorporating an objective with a high numerical aperture, spot sizes of 10−20 μm were readily achieved. As few as five adherent cells could be specifically selected for analysis in their culturing environment. The importance of in situ analysis was highlighted by comparing the metabolite composition of adherent versus suspended cells. For example, we observed that cells analyzed adherently yielded higher values for the adenylate energy charge (0.90 ± 0.09 for adherent cells vs 0.09 ± 0.03 for suspended cells). Additionally, due to the smaller focal spot size, tg-LAESI enabled the analysis of ∼20 times smaller cell populations compared to rg-LAESI.

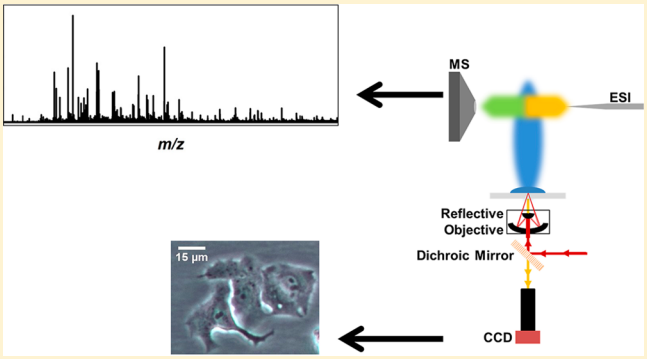

Cell cultures have long been used to provide insight into human health and disease.[1−3] Metabolomic analysis of cultured cells is limited by cell preparation processes that require quenching, lysing, and detachment of cells from these surfaces (e.g., trypsinization or scraping).[4,5] Due to scant alternatives, these sample preparation steps are widely used to measure metabolites in cells despite the onset of potential artifacts due to rapid metabolic changes.[6,7]

Recently, there have been investigations into optimizing protocols by varying the harvesting and extraction conditions.[8] However, there have been few attempts to evaluate the effects of these techniques on the metabolic makeup of cells.[9−12]

Traditional adherent mammalian cell cultures rely on the adhesion of cells and extra-cellular matrix to an artificial surface.[13] Recent studies have also begun to delve into the highly complex extra-cellular matrix (ECM) and its effects on the nature of cell morphology.[14,15] Based on the physical and chemical characteristics of the surface that cells adhere to, they exhibit morphological properties more or less similar to their in vivo counterparts.[16] Meanwhile, few biochemical methods are currently capable of measuring the broad metabolic changes due to adhesion, because of the sample preparation requirements.[17]

Small groups of cells often play specific roles in metabolism within a tissue for a wide array of organisms and require an appropriate technique for isolation and analysis. In plants, for example, symbiotic relationships can form between organisms, resulting in the formation of small substructures or nodules that can have a significant effect in nitrogen fixation.[18] Among tumors, there can be highly heterogeneous distribution of cells, often with only certain subsets giving rise to future metastases.[19] Within the human pancreas, the islets of Langerhans can play critical roles in the metabolic network, often requiring islets to be analyzed separately from the surrounding tissue.[20,21]

Sample preparations for metabolomic analysis are necessary for standard techniques, such as high-performance liquid chromatography (HPLC), and are inherently not conducive to analyzing cells in their native environment.[22,23] Matrix-assisted laser desorption ionization (MALDI) and C_{60} secondary ion mass spectrometry (SIMS) have been utilized to investigate intact cells.[24,25] These techniques are well suited to analyze metabolite species that are either high or low in mass, respectively, but there is room for a complementary technique

Received: August 3, 2015
Accepted: November 11, 2015
Published: November 11, 2015

DOI: 10.1021/acs.analchem.5b02971
Anal. Chem. 2015, 87, 12130−12136

to address a broader range of metabolites. Traditional MALDI relies on matrix cocrystallization for ion formation, which can disrupt cell integrity, in addition to requiring a high vacuum for analysis.[26] Ambient ionization methods, such as desorption electrospray ionization (DESI) can be used to analyze cell cultures after some sample preparation.[27,28]

Several of these techniques have also been configured in the so-called transmission geometry (tg) configuration. In tg laser ablation or desorption experiments, the beam is incident on the reverse side of the sample.[29−32] Ions generated from MALDI in tg were found to be similar to those observed in reflection geometry experiments.[33] Similarly, tg DESI experiments produced meaningful spectra.[34] Current high-resolution MALDI imaging relies heavily on improved optics that can only be used in the tg arrangement due to their physical specifications, including focal length.[35] Laser ablation electrospray ionization (LAESI) mass spectrometry (MS) has previously been used for analysis of mammalian cells and tissues.[36−38] In these reflection geometry (rg) studies, rg-LAESI had a laser spot size of 150−300 μm in diameter and the laser beam impinged on the same side of the sample as the ejection of ablation plume.[39] Later LAESI was adapted to include ablation via an etched optical fiber, allowing smaller spot sizes of 30−40 μm that enabled single plant cell analysis.[40] The optical fiber, however, may decrease sensitivity due to a partial blockage of the ejected plume by the physical proximity of the fiber.

By adapting the sampling process of LAESI to tg mode, a lens with a higher numerical aperture and correspondingly shorter working distance can be used. Depending on sample characteristics, the spot size was lowered to 10−40 μm, a significant reduction compared to conventional rg-LAESI. Here we describe the utility of tg-LAESI for analysis of small populations of live adherent cells coupled with real-time microscope observation.

EXPERIMENTAL SECTION

Chemicals. HPLC-grade water, methanol, and chloroform were purchased from Alfa Aesar (Ward Hill, MA), and glacial acetic acid was obtained from Riedel-de Haën (Seelze, Germany). Rhodamine 6G was acquired from Fluka (St. Louis, MO). All stock solutions were prepared in HPLC grade water.

Cell Culture. A cryogenic stock of HepG2/C3A cells (ATCC, Manassas, VA), epithelial cells derived from a hepatocellular carcinoma, were used for all experiments. Cells were maintained in Eagle's Minimum Essential Medium (EMEM) medium, supplemented with 10% fetal bovine serum and 1% penicillin-streptomycin. While not being analyzed, all cultures were maintained in a 5% CO_2, humidity-controlled incubator (HeraCell, Thermo Scientific, Waltham, MA). All experiments were performed on cells that had been seeded at least 48 h prior to analysis on ethanol-sterilized, untreated glass microscope slides (VWR Micro Slides, VWR, Radnor, PA) within a 10 cm polystyrene Petri dish, as part of the regular cell culturing process, with a density that allowed for the surface to be ∼50−70% covered initially. For suspended cell experiments, similar concentrations of cells were seeded in a T75 flask and maintained at 37 °C with 5% CO_2 at constant humidity.

Sample Preparation. For adherent cell analysis, cells were washed with 5−10 mL room temperature deionized (DI) water prior to analysis. Excess water was removed by keeping the slide vertical for ∼15 s, and the back of the slide was dried to eliminate the absorption of the laser light by water residues. The cells were analyzed within 1 min. For suspended cell analysis, cells were washed with 1× HyClone PBS (Fisher Scientific, Fair Lawn, NJ) at room temperature. Cells were detached without tapping by adding 2 mL of ∼37 °C 0.25× trypsin-EDTA (Life Technologies, Carlsbad, CA). After cells detached, usually within 4 to 8 min, 2 mL of PBS buffer was added to the cell suspension and centrifuged at 1000*g* for 2 min. After discarding the PBS, the cell pellet was resuspended with complete medium. To obtain a cell pellet for LAESI analysis, aliquots of 1 mL (10^6 cells/mL) were centrifuged at 1000*g*, resuspended in deionized water to avoid interfering buffer-related ions, and centrifuged again at 1000*g* for 2 min. Immediately prior to LAESI analysis, cell pellets were resuspended in 15−30 μL of DI water and pipetted onto a sample holder. Cells were counted using an automated cell counter (Countess, Invitrogen, Eugene, OR) before obtaining a pellet.

Reflection and Transmission Geometry LAESI. Details of the conventional rg-LAESI system have been described earlier.[41] In the tg-LAESI experiments, a Nd:YAG optical parametric oscillator (Vibrant, Opotek, Carlsbad, CA) with a 4 ns pulse width, tuned to 2.94 μm wavelength, operating at 10 Hz, produced a beam with a diameter of ∼3 mm. Beam diameter was measured at the laser cavity exit using a liquid crystal thermal card (VRC6, Thorlabs, Newton, NJ). The beam was directed using gold mirrors and a dichroic mirror (DMSP805, Thorlabs, Newton, NJ) that directed the beam through the 40× reflective objective (LMM-40X-P01, Thorlabs, Newton, NJ). Due to the low reflectance of the dichroic mirror (∼20%) as well as silver broadband coating on the reflective objective, higher laser energy was required for the tg experiments. Visible light was transmitted through the dichroic mirror from the cell sample to the tube lens (7× precision zoom, Edmund Optics, Barrington, NJ) and captured by a CMOS camera (DCC3240C, Thor Laboratories, Newton, NJ). Coupling of the reflective objective with dichroic mirror enabled simultaneous ablation and visualization of adherent cells. Mechanical vibration was reduced by increasing the flexural rigidity of the optical system mounted on a vertical breadboard. The sample holder was positioned by a 3-axis translation stage to allow for precise control. The reflective objective also required a translation stage to achieve precise focusing due to its narrow depth of focus. See the schematic of top view in Figure 1. The angle (θ = 90°) of the vertical breadboard and placement of the ablation spot halfway between the mass spectrometer orifice and the tip of the electrospray emitter (w/2) proved to be ideal for optimal signal (see Figure 1).

For either configuration of LAESI, the plume of neutrals was captured by a home-built electrospray system. The spray geometry remained unchanged but the ablation geometry was modified to optimize the ion signal (see later). This electrospray setup has been described previously.[41] Briefly, electrospray solution was supplied by syringe pump (Physio 22, Harvard Apparatus, Holliston, MA) with a flow rate of 400 nL/min through a tapered tip stainless steel emitter (ID = 100 μm, MT320-100-5-5, New Objective Inc., Woburn, MA), positioned about 10 mm away from the mass spectrometer orifice. For positive ion mode, a solution of 1:1 methanol/water with 0.1% acetic acid (v/v) was supplied, whereas for negative ion mode, a solution of 2:1 methanol/chloroform with 0.1% acetic acid (v/v) was used. The emitter was connected to a high voltage power supply (PS350, Sanford Research Systems, Sunnyvale, CA), operating at +3300 or −2400 V, in the two modes, respectively.

All MS measurements were acquired using a Q-TOF mass spectrometer (Q-TOF Premiere, Waters Co., Milford, MA) in single reflectron mode. With a lock-mass for an internal calibrant

DOI: 10.1021/acs.analchem.5b02971
Anal. Chem. 2015, 87, 12130−12136

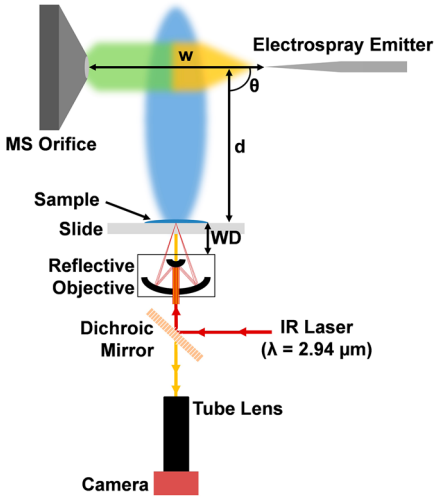

Figure 1. Schematic of tg-LAESI showing the interception of the ablation plume by the electrospray. Optimal parameters for MS signal included the angle between the axes of the two plumes (θ = 90°) and electrospray emitter (ESI) to sample distance (d = 19 mm). Focusing of the dual use reflective objective, with a working distance (WD) of 7.8 mm, for ablation was achieved by adjusting for a sharp microscope image. The sample ablation was positioned at half the distance (w) between the ESI emitter tip and the MS orifice for optimal signal intensity.

(reduced glutathione), the mass accuracy of the Q-TOF Premiere was ~5 mDa. Data was acquired and processed using MassLynx (Version 4.1, Waters Co., Milford, MA). Selected ions of interest were fragmented using collision induced dissociation (CID) with a collision cell pressure of ~8.73×10^{-3} mbar and collision energies in the 5−30 eV range.

Data Analysis. Tandem MS spectra were verified using matches found in the METLIN database (Scripps, La Jolla, CA, https://metlin.scripps.edu/index.php, last accessed July 17, 2015).[42] Spot sizes were characterized using thermal paper (Résiste 600-7.5, Appleton Papers, Inc., Appleton, WI). Burn marks were subsequently imaged using bright-field light microscopy, and processed using ImageJ (Version 1.48, National Institutes of Health, U.S.A.). This image processing included thresholding the images into binary and using the "Analyze Particles" command, which scans the binarized image for objects and records their area. As there was minimal deviation in shape, all laser spots were assumed to be perfectly circular with areas provided by ImageJ. Areas were then converted to diameters to provide a more meaningful measure of focusing capabilities.

RESULTS AND DISCUSSION

Enhanced Focusing and Improved Limit of Detection. To improve the focusing of the laser beam originating from the OPO, a high numerical aperture lens was required. A composite microscope objective lens with a numerical aperture of NA = 0.5 and a working distance of WD = 7.8 mm offered a 10-fold improvement in NA over the single element plano-convex lens used in rg-LAESI. As the selected lens was based on reflective optics, it was also free of chromatic aberration. Installing the optical system on a vertical breadboard reduced the vibration of the focusing and imaging components through enhanced flexural rigidity. These improvements resulted in a reduced focal spot size. Focusing performance was measured over a range of energies for single laser pulses using thermal paper. Overall, the spot size slightly increased with growing pulse energy (see Figure S1 in the Supporting Information). For fluences below 2.5 J/cm^2, the ablation spot size was 8.4 ± 3.2 μm (n = 5), whereas at the maximum laser fluence of 5.6 J/cm^2, it reached 18.9 ± 0.5 μm (n = 5). The laser energy used for cell ablation experiments was ~5.0 mJ, corresponding to ~4.7 J/cm^2. Although submicrometer ablation spots produced by a UV laser have been demonstrated in the literature,[43] those results cannot be directly compared to the tg-LAESI arrangement. The OPO system used in the LAESI-MS experiments produces a highly divergent beam resulting in a focal spot size significantly exceeding the diffraction limit.

In LAESI-MS, reducing the focal spot size limits the amount of ablated material available for analysis. To determine if this limited amount of material could be detected, solid rhodamine 6G was analyzed using the newly installed optical system. Analysis by tg-LAESI-MS from a 10 μm ablated spot yielded an M$^+$ peak with S/N > 3 for rhodamine 6G. Once all ablation and spray geometry parameters were optimized, limit of detection (LOD) curves were established for tg-LAESI using rhodamine 6G, leucine encephalin, and reduced glutathione standard solutions plotting ion intensities as a function of the ablated amount per 10 laser pulses (see Figure 2). The LOD for rhodamine 6G was 300 amol,

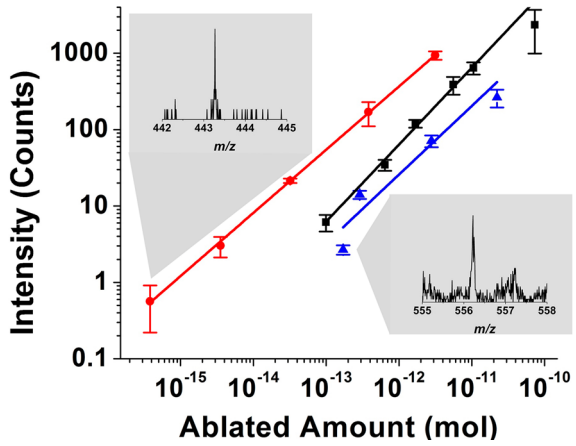

Figure 2. Ion intensities as a function of sample amount ablated by 10 laser pulses in tg-LAESI of rhodamine 6G (red ●), reduced glutathione (■), and leucine enkephalin (blue ▲) solutions. The limits of detection for these compounds were 300 amol, 100 fmol, and 170 fmol, respectively.

whereas leucine encephalin had an LOD of 170 fmol, and glutathione exhibited an LOD of 100 fmol. The dynamic range for positive ion detection, based on the glutathione and leucine encephalin data was 2 to 3 orders of magnitude (see Figure 2).

We observed that the ion yield in tg-LAESI increased as the distance between the sample and electrospray axis approached 16 mm and saturated at ~19 mm (see Figure S2 in the Supporting Information). Compared to rg-LAESI, where a distance of ~15 mm yielded optimal signal, this observation indicated a slightly extended range for the ablated particles.[44] Ablation in this configuration does impose a limit on sample thickness of up to ~30 μm. This is not a significant limitation for fresh frozen tissue sections or adherent monolayers of cells.

Targeting and Ablation of Adherent Cells. With the tg configuration, the culturing surface has to transmit at both mid-IR and visible wavelengths in order to ablate and observe the sample. Thus, cells were cultured on 1 mm thick glass microscope slides. Previous observations indicated that laser irradiation in tg can cause catapulting of entire cells without ablating them to produce a plume.[45] Once adhered to the glass

DOI: 10.1021/acs.analchem.5b02971
Anal. Chem. 2015, 87, 12130−12136

slide surface, cells could be visualized and targeted during the ablation process. With the improved focusing afforded in tg-LAESI, targeting of individual human cells became possible. However, the sensitivity of the detection was insufficient to generate mass spectra from single cells. Small populations of cells were analyzed by tg-LAESI-MS, and microscope visualization allowed correlation of the signal with the number and types of cells sampled.

Analysis of Small Adherent Cell Populations by tg-LAESI-MS. For the cells cultured on the microscope slides, tg-LAESI was employed for metabolic analysis of small cell populations (n = 5 to 100). The diameter of the ablated area, typically 30 to 40 μm, could be varied by adjusting the position of the focusing lens and/or the energy of the laser pulse. Although the initial experiments with rhodamine 6G samples indicated ~10 μm ablation spots, in situ ablation of cellular monolayers required higher laser pulse energies resulting in larger ablation marks. A typical positive ion mass spectrum of five adherent cells (see inset) obtained from tg-LAESI is shown in Figure 3, with six

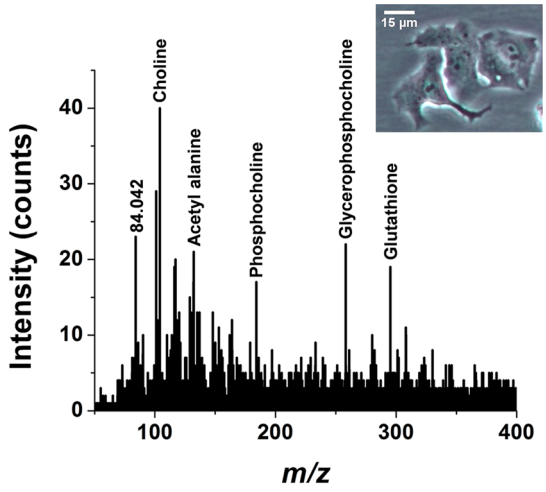

Figure 3. Positive ion tg-LAESI mass spectrum of five mammalian cells. The inset shows an optical image of five hepatocytes through the long distance microscope.

metabolites marked. The six peaks were identified using accurate mass, isotopic distribution, and MS/MS analysis of large cell groups with rg-LAESI for confirmation (see Table 1). In total, there were ~20 cell-related peaks in this spectrum, as determined by tracking each ion as cell numbers decreased, including those of unidentified ions. With the ability of detecting 20 molecular features from only 5 cells, tg-LAESI could be used to provide relatively robust information with very little sample.

Figure 4A demonstrates the variation of molecular coverage with the reduction in the number of cells analyzed. The 1000 cell spectrum contains at least 66 cell related peaks, and the 100 cell spectrum has 40, with the lower cell numbers (n = 10 and 25) each containing 15−20 peaks. This decrease in molecular coverage is expected but could be improved by incorporating ion separation using an ion mobility separation step.[46,47] In 1000 cells, the observed ~5 lipid species were likely identical to the phosphatidylcholines identified in large cell populations (~10^6 cells). In less than 1000 cells, there were only metabolites (m/z < 500) observed. As expected, the signal-to-noise ratio decreased with each successive reduction in the number of cells (see Figure 4A). Similarly, a decrease in molecular coverage was observed with fewer cells analyzed, in part due to the differences in relative ionization efficiencies of the various metabolites. Unlike the easy to ionize metabolites listed in Table 1 that were observed even at very low cell numbers, other species, such as hexoses, were only observed in the mass spectra of larger cell populations. The signal-to-noise ratio (S/N) of the 1000 cell spectrum (top) was about 180, followed by 56, 22, and 10 as the analyzed number of cells decreased. For some peaks, the S/N became marginal at the 10 cell level, although there were a similar number of molecular features observed in the 25 and 10 cell spectra.

In Figure 4B, the intensities of certain peaks in the tg-LAESI spectra are followed as the function of the analyzed cell population size. In the 10 to 1000 cell range, as the cell number decreased the signal intensity of the selected ions decreased proportionally. The slope in all cases ranged from 0.73 (glutathione) to 1.3 (choline), and almost all R^2 values were >0.95, except for phosphocholine, which was 0.74.

Adenylate Energy Charge Measured Using tg-LAESI-MS. In negative ion mode, adenosine di- and triphosphate (ADP and ATP, respectively) were commonly detected, but the monophosphate (AMP) was sparsely observed. Experiments with ATP, ADP, and AMP standards indicated the presence of in-source decay for ATP and AMP. Decomposition of 43% of the former produced ADP, whereas a 15% decomposition of the latter resulted in the production of a fragment ion with nominal m/z 211. The ionization efficiencies for the three compounds were similar, so not observing AMP in the cell spectra indicated that its level in the cells was below the limit of detection.

Groups of 20−50 adherent cells were sampled and the ion intensities for ATP, ADP, and AMP, varied in the resulting spectra (see Figure 5 and for identification Table 2). These changes were reflected in the adenylate energy charge (AEC) calculated using the integrated ion intensities, following the AEC = (0.5ADP + ATP)/(AMP + ADP + ATP) formula. Ion intensities were corrected for the effect of in-source decomposition. The AEC values range between 0 and 1 and are used to characterize cell health. For healthy cells, the values are typically AEC > 0.5. Although the form of cell death through apoptosis, necrosis or autophagy depends on multiple factors, under certain conditions, ATP levels and the related AEC have been shown to

Table 1. List of Positive Ions Detected by tg-LAESI from Five Cells and Identified by rg-LAESI Using Tandem MS

name	formula	m/z_{meas}	m/z_{calc}	Δm (mDa)	MS/MS ions[b]
acetyl alanine	$[C_5H_9NO_3+H]^+$	132.075	132.066	9	114, 90, 86
choline	$[C_5H_{13}NO+H]^+$	104.105	104.108	3	60
pyroglutamic acid	$[C_5H_7NO_3+H]^+$	130.047	130.050	3	84
phosphocholine	$[C_5H_{14}NO_4P+H]^+$	184.070	184.074	4	125, 99, 86
glycerophosphocholine	$[C_8H_{20}NO_6P+H]^+$	258.092	258.111	19	184, 129, 104
glutathione, reduced	$[C_{10}H_{17}N_3O_6S+H]^+$	308.092	308.092	0[a]	290, 245, 233, 215, 179, 162, 144, 142, 130, 116, 84, 76

[a]Used as internal lock-mass calibrant. [b]Obtained from large cell populations by rg-LAESI.

DOI: 10.1021/acs.analchem.5b02971
Anal. Chem. 2015, 87, 12130−12136

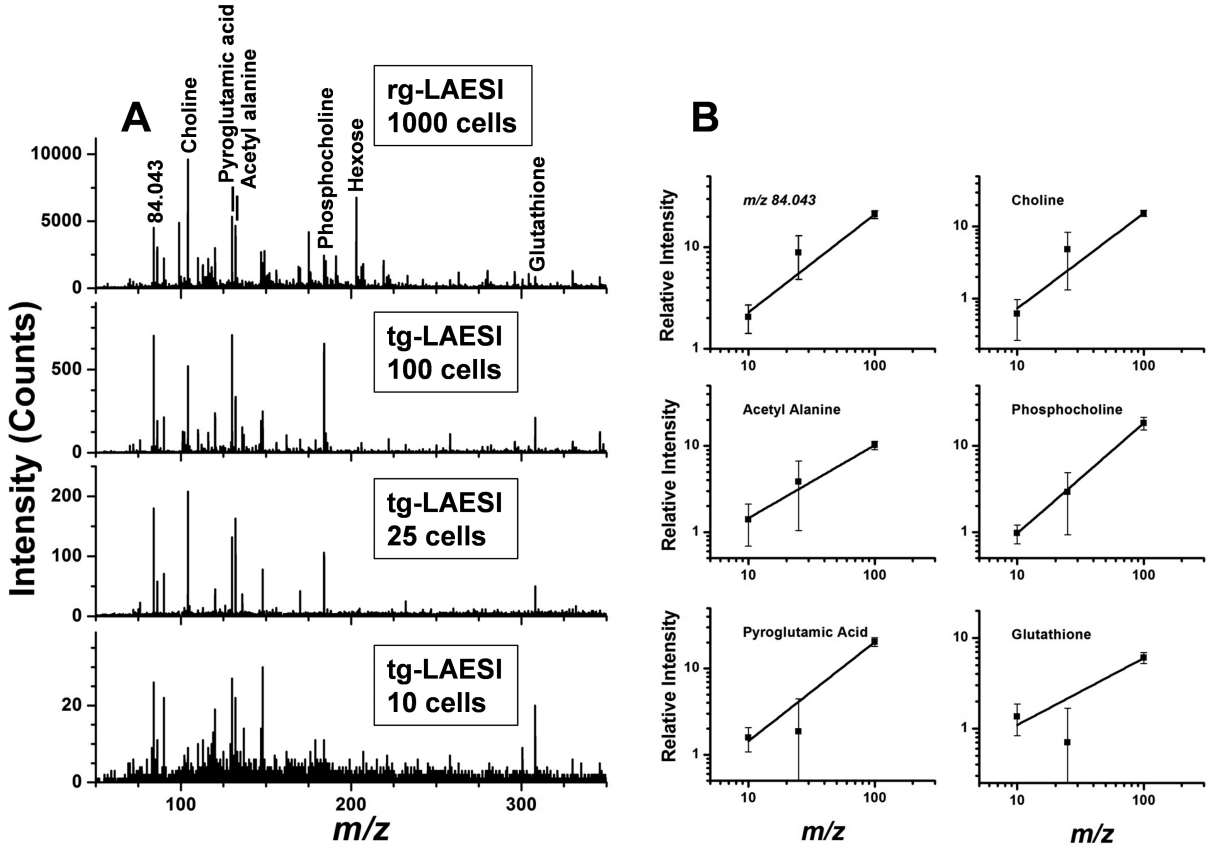

Figure 4. (A) Comparison of an rg-LAESI spectrum of 1000 cells (top) with tg-LAESI mass spectra of ~100, 25, and 10 adherent cells (below). (B) Relative ion intensities as a function of cell numbers are shown for selected metabolites.

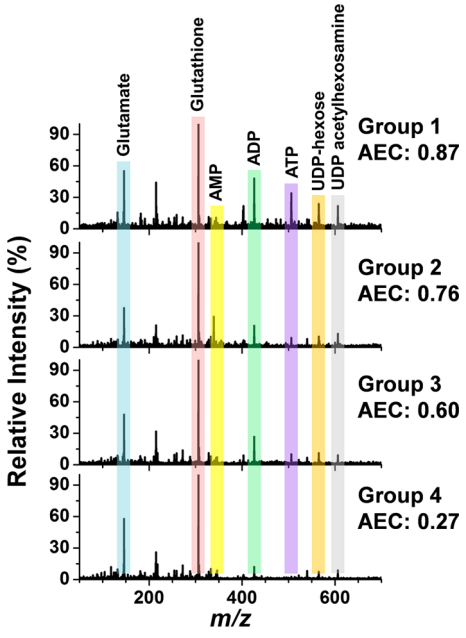

Figure 5. Negative ion mode tg-LAESI mass spectra for four groups of 20−50 adherent hepatocytes. Smoothed and integrated peak areas were represented by bars. The adenylate energy charge (AEC) is indicated for each group.

have a decisive influence.[48] When the AEC < 0.5, lower values are typically associated with necrosis and higher readings indicate apoptosis. Three of the four cell groups in Figure 5 exhibited AEC values above 0.5 ranging from 0.60 to 0.87. The fourth cell group with AEC = 0.27 represented cells undergoing apoptosis or necrosis. Other ion intensities, including glutamate, glutathione, and UDP-hexose, stayed relatively constant across cell groups.

Comparing adherent and pelleted cells, there was a clear increase in the relative sensitivity for low mass ions that resulted in ~10× higher ion counts in both polarities for similar numbers of cells. This may be due to the increased sampling efficiency for adherent cells during ablation, evidenced by a minimal amount of remaining cell debris after the analysis.

In positive ion mode, phosphatidylcholines were scarcely observed in adherent cells, whereas spectra from suspended cells appeared to be richer in these ions. In negative ion mode, however, there were similar molecular features under both analysis conditions.

In negative ion mode rg-LAESI analysis of suspended cells, AMP and ADP were routinely detected, whereas ATP was seldom observed (see the bottom spectrum in Figure S3). In contrast, ATP was reliably detected from adherent cell populations (see the top spectrum in Figure S3). In addition, there was a large decrease in the intensity of AMP. Indeed, the rg-LAESI and tg-LAESI of adherent cells produced similar ions and relative intensities for adenylates. The AEC was found to be 0.90 ± 0.09 for tens to hundreds of thousands of adherent cells, whereas suspended cells had an AEC of 0.09 ± 0.03, further suggesting the healthier status of adherent cells.

The marginal levels of ATP signal in the rg-LAESI spectra of suspended cells might be due to the extensive sample preparation process. Typical cell pellet analysis required cell detachment by

DOI: 10.1021/acs.analchem.5b02971
Anal. Chem. 2015, 87, 12130−12136

Table 2. List of Negative Ions Detected by tg-LAESI from 20−50 Hepatocytes and Identified by rg-LAESI Using Tandem MS

name	formula	m/z_{meas}	m/z_{calc}	Δm (mDa)	MS/MS ions[b]
glutamate	$[C_5H_9NO_4-H]^-$	146.046	146.045	1	128, 102, 84
glutathione, reduced	$[C_{10}H_{17}N_3O_6S-H]^-$	306.076	306.076	0[a]	288, 272, 254, 210, 179, 160, 143, 128, 99
AMP	$[C_{10}H_{14}N_5O_7P-H]^-$	346.058	346.055	3	211, 193, 151, 134, 97, 79
ADP	$[C_{10}H_{15}N_5O_{10}P_2-H]^-$	426.025	426.022	3	408, 328, 291, 273, 159, 134, 97, 79
ATP	$[C_{10}H_{16}N_5O_{13}P_3-H]^-$	505.993	505.988	5	426, 408, 273, 177, 159, 79
UDP-hexose	$[C_{15}H_{24}N_2O_{17}P_2-H]^-$	565.047	565.060	13	403, 385, 323, 241, 211, 159, 97, 79
UDP-acetylhexosamine	$[C_{17}H_{27}N_3O_{17}P_2-H]^-$	606.074	606.085	11	526, 403, 385, 362, 344, 323, 282, 273, 177, 159, 111, 97, 79

[a]Used as internal lock-mass calibrant. [b]Obtained from large cell populations by rg-LAESI.

trypsinization and longer washing steps that might be sufficient to induce metabolic changes. In contrast, the analysis of adherent cells required no trypsinization or scraping for detachment and reported significantly higher ATP levels. When compared with trypsinization, increased ATP levels in direct metabolite extraction have been observed previously by HPLC.[49]

We found that the ATP signal was higher from adherent cells, and there was also a marked reduction in AMP intensities that contributed to the observation of increased energy charge in both rg-LAESI and tg-LAESI analysis. The latter, however, provided enhanced capabilities for cell targeting and local analysis of small groups of cells.

CONCLUSIONS

Small populations (n = 5 to 100) of adherent mammalian cells were analyzed using tg-LAESI, in situ, without significant sample preparation. The differences between cells analyzed adherently and in suspension were exemplified by the significantly higher abundance of ATP, likely due to the absence of trypsinization and additional washing steps. Due to the reduced sample processing needs, analysis of adherent cells captured a less distorted biochemical cell composition compared to suspended equivalents. In addtion, the higher signal intensity observed for adherent cells could be helpful when analyzing a limited number of cells or studying cellular heterogeneity. In the future, the introduction of gas-phase ion mobility separation can both increase the coverage of biomolecules, as well as enhance the S/N, with the ultimate goal of single-cell analysis.

As a result of the integrated optical imaging capability, tg-LAESI has enables the selection of cells based on their morphology or phenotype. Moreover, special surface treatments that promote morphological similarities between cultured and primary cells could be combined with this technique to observe their biochemical differences. In order to improve the spatial resolution of the optical images, tg-LAESI can be combined with a research-grade microscope by mounting the sample on the microscope stage. Potential applications of tg-LAESI analysis of small adherent cell populations include differentiating cell phenotypes in disease states, pharmacokinetic studies in select subpopulations of sorted cells, and studying the interactions of cocultured cells.

ASSOCIATED CONTENT

Supporting Information

The Supporting Information is available free of charge on the ACS Publications website at DOI: 10.1021/acs.analchem.5b02971.

Supplemental data including spot diameters as function of laser energy output, distance-dependent signal intensity, and rg-LAESI-MS spectra (PDF)

AUTHOR INFORMATION

Corresponding Author

*E-mail: vertes@gwu.edu. Phone: +1 (202) 994-2717. Fax: +1 (202) 994-5873.

Notes

The authors declare no competing financial interest.

ACKNOWLEDGMENTS

The authors acknowledge financial support by the U.S. Department of Energy, Office of Basic Energy Sciences, Chemical Sciences, Geosciences, and Biosciences Division under Award DE-FG02-01ER15129 and the GW Selective Excellence Fund.

REFERENCES

(1) Otterbein, L. E.; Bach, F. H.; Alam, J.; Soares, M.; Lu, H. T.; Wysk, M.; Davis, R. J.; Flavell, R. A.; Choi, A. M. K. *Nat. Med.* **2000**, *6*, 422−428.
(2) Park, I.-H.; Arora, N.; Huo, H.; Maherali, N.; Ahfeldt, T.; Shimamura, A.; Lensch, M. W.; Cowan, C.; Hochedlinger, K.; Daley, G. Q. *Cell* **2008**, *134*, 877−886.
(3) Bild, A. H.; Yao, G.; Chang, J. T.; Wang, Q. L.; Potti, A.; Chasse, D.; Joshi, M. B.; Harpole, D.; Lancaster, J. M.; Berchuck, A.; Olson, J. A.; Marks, J. R.; Dressman, H. K.; West, M.; Nevins, J. R. *Nature* **2006**, *439*, 353−357.
(4) Alvarez-Sanchez, B.; Priego-Capote, F.; de Castro, M. D. L. *TrAC, Trends Anal. Chem.* **2010**, *29*, 120−127.
(5) Halama, A. *Arch. Biochem. Biophys.* **2014**, *564*, 100−109.
(6) Chokkathukalam, A.; Kim, D.-H.; Barrett, M. P.; Breitling, R.; Creek, D. J. *Bioanalysis* **2014**, *6*, 511−524.
(7) You, L.; Zhang, B.; Tang, Y. J. *Metabolites* **2014**, *4*, 142−165.
(8) Ser, Z.; Liu, X.; Ngoc Nu, T.; Locasale, J. W. *Anal. Biochem.* **2015**, *475*, 22−28.
(9) Dettmer, K.; Nurnberger, N.; Kaspar, H.; Gruber, M. A.; Almstetter, M. F.; Oefner, P. J. *Anal. Bioanal. Chem.* **2011**, *399*, 1127−1139.
(10) Bi, H.; Krausz, K. W.; Manna, S. K.; Li, F.; Johnson, C. H.; Gonzalez, F. J. *Anal. Bioanal. Chem.* **2013**, *405*, 5279−5289.
(11) Hutschenreuther, A.; Kiontke, A.; Birkenmeier, G.; Birkemeyer, C. *Anal. Methods* **2012**, *4*, 1953−1963.
(12) Lorenz, M. A.; Burant, C. F.; Kennedy, R. T. *Anal. Chem.* **2011**, *83*, 3406−3414.
(13) Ratner, B. D.; Bryant, S. J. *Annu. Rev. Biomed. Eng.* **2004**, *6*, 41−75.
(14) Ho, F. C.; Zhang, W.; Li, Y. Y.; Chan, B. P. *Biomaterials* **2015**, *53*, 392−405.
(15) Kyle, D. J. T.; Oikonomou, A.; Hill, E.; Bayat, A. *Biomaterials* **2015**, *52*, 88−102.
(16) Herrema, H.; Czajkowska, D.; Theard, D.; van der Wouden, J. M.; Kalicharan, D.; Zolghadr, B.; Hoekstra, D.; Ijzendoorn, S. C. D. *Mol. Biol. Cell* **2006**, *17*, 3291−3303.
(17) Arkesteijn, I. T.; Smolders, L. A.; Spillekom, S.; Riemers, F. M.; Potier, E.; Meij, B. P.; Ito, K.; Tryfonidou, M. A. *Arthrit. Res. Ther.* **2015**, *17*, 569−569.

DOI: 10.1021/acs.analchem.5b02971
Anal. Chem. 2015, 87, 12130−12136

(18) Ye, H.; Gemperline, E.; Venkateshwaran, M.; Chen, R.; Delaux, P.-M.; Howes-Podoll, M.; Ane, J.-M.; Li, L. *Plant J.* **2013**, *75*, 130−145.
(19) Gerlinger, M.; Rowan, A. J.; Horswell, S.; Larkin, J.; Endesfelder, D.; Gronroos, E.; Martinez, P.; Matthews, N.; Stewart, A.; Tarpey, P.; Varela, I.; Phillimore, B.; Begum, S.; McDonald, N. Q.; Butler, A.; Jones, D.; Raine, K.; Latimer, C.; Santos, C. R.; Nohadani, M.; Eklund, A. C.; Spencer-Dene, B.; Clark, G.; Pickering, L.; Stamp, G.; Gore, M.; Szallasi, Z.; Downward, J.; Futreal, P. A.; Swanton, C. *N. Engl. J. Med.* **2012**, *366*, 883−892.
(20) Ohtani, O. *Archivum Histologicum Japonicum* **1987**, *50*, 557−566.
(21) Perl, A. K.; Wilgenbus, P.; Dahl, U.; Semb, H.; Christofori, G. *Nature* **1998**, *392*, 190−193.
(22) del Val, I. J.; Kyriakopoulos, S.; Polizzi, K. M.; Kontoravdi, C. *Anal. Biochem.* **2013**, *443*, 172−180.
(23) Dietmair, S.; Hodson, M. P.; Quek, L.-E.; Timmins, N. E.; Chrysanthopoulos, P.; Jacob, S. S.; Gray, P.; Nielsen, L. K. *Biotechnol. Bioeng.* **2012**, *109*, 1404−1414.
(24) Lanni, E. J.; Dunham, S. J. B.; Nemes, P.; Rubakhin, S. S.; Sweedler, J. V. *J. Am. Soc. Mass Spectrom.* **2014**, *25*, 1897−1907.
(25) Zimmerman, T. A.; Rubakhin, S. S.; Sweedler, J. V. *J. Am. Soc. Mass Spectrom.* **2011**, *22*, 828−836.
(26) Zhang, X.; Scalf, M.; Berggren, T. W.; Westphall, M. S.; Smith, L. M. *J. Am. Soc. Mass Spectrom.* **2006**, *17*, 490−499.
(27) Bodzon-Kulakowska, A.; Drabik, A.; Marszalek, M.; Kotlinska, J. H.; Suder, P. *J. Mass Spectrom.* **2014**, *49*, 613−621.
(28) Watrous, J. D.; Dorrestein, P. C. *Nat. Rev. Microbiol.* **2011**, *9*, 683−694.
(29) Galicia, M. C.; Vertes, A.; Callahan, J. H. *Anal. Chem.* **2002**, *74*, 1891−1895.
(30) Richards, A. L.; Lietz, C. B.; Wager-Miller, J. B.; Mackie, K.; Trimpin, S. *Rapid Commun. Mass Spectrom.* **2011**, *25*, 815−820.
(31) West, R. E., III; Findsen, E. W.; Isailovic, D. *J. Am. Soc. Mass Spectrom.* **2013**, *24*, 1467−1476.
(32) Wechsung, R.; Hillenkamp, F.; Kaufmann, R.; Nitsche, R.; Vogt, H. *Scan. Electron Microsc.* **1978**, *1*, 611−620.
(33) Vertes, A.; Balazs, L.; Gijbels, R. *Rapid Commun. Mass Spectrom.* **1990**, *4*, 263−266.
(34) Chipuk, J. E.; Brodbelt, J. S. *J. Am. Soc. Mass Spectrom.* **2008**, *19*, 1612−1620.
(35) Zavalin, A.; Todd, E. M.; Rawhouser, P. D.; Yang, J. H.; Norris, J. L.; Caprioli, R. M. *J. Mass Spectrom.* **2012**, *47*, 1473−1481.
(36) Sripadi, P.; Shrestha, B.; Easley, R. L.; Carpio, L.; Kehn-Hall, K.; Chevalier, S.; Mahieux, R.; Kashanchi, F.; Vertes, A. *PLoS One* **2010**, *5*, e12590.
(37) Nemes, P.; Woods, A. S.; Vertes, A. *Anal. Chem.* **2010**, *82*, 982−988.
(38) Shrestha, B.; Sripadi, P.; Walsh, C. M.; Razunguzwa, T. T.; Powell, M. J.; Kehn-Hall, K.; Kashanchi, F.; Vertes, A. *Chem. Commun.* **2012**, *48*, 3700−3702.
(39) Li, H.; Smith, B. K.; Mark, L.; Nemes, P.; Nazarian, J.; Vertes, A. *Int. J. Mass Spectrom.* **2015**, *377*, 681−689.
(40) Shrestha, B.; Vertes, A. *Anal. Chem.* **2009**, *81*, 8265−8271.
(41) Nemes, P.; Vertes, A. *Anal. Chem.* **2007**, *79*, 8098−8106.
(42) Smith, C. A.; O'Maille, G.; Want, E. J.; Qin, C.; Trauger, S. A.; Brandon, T. R.; Custodio, D. E.; Abagyan, R.; Siuzdak, G. *Ther. Drug Monit.* **2005**, *27*, 747−751.
(43) Zavalin, A.; Yang, J. H.; Haase, A.; Holle, A.; Caprioli, R. *J. Am. Soc. Mass Spectrom.* **2014**, *25*, 1079−1082.
(44) Nemes, P.; Huang, H.; Vertes, A. *Phys. Chem. Chem. Phys.* **2012**, *14*, 2501−2507.
(45) Schutze, K.; Lahr, G. *Nat. Biotechnol.* **1998**, *16*, 737−742.
(46) Shrestha, B.; Vertes, A. *Anal. Chem.* **2014**, *86*, 4308−4315.
(47) Zhang, L.; Vertes, A. *Anal. Chem.* **2015**, *87*, 10397−10405.
(48) Eguchi, Y.; Shimizu, S.; Tsujimoto, Y. *Cancer Res.* **1997**, *57*, 1835−1840.
(49) Yang, M. S.; Gupta, R. C. *Toxicol. Mech. Methods* **2003**, *13*, 97−101.

DOI: 10.1021/acs.analchem.5b02971
Anal. Chem. 2015, 87, 12130−12136

Supporting Information

for

In Situ Analysis of Small Populations of Adherent Mammalian Cells Using Laser Ablation Electrospray Ionization Mass Spectrometry in Transmission Geometry

Rachelle S. Jacobson, Richard Thurston, Bindesh Shrestha, and Akos Vertes*

Department of Chemistry, W. M. Keck Institute for Proteomics Technology and Applications, The George Washington University, Washington, DC 20052

*To whom correspondence should be addressed. E-mail: vertes@gwu.edu. Phone: +1 (202) 994-2717. Fax: +1 (202) 994-5873

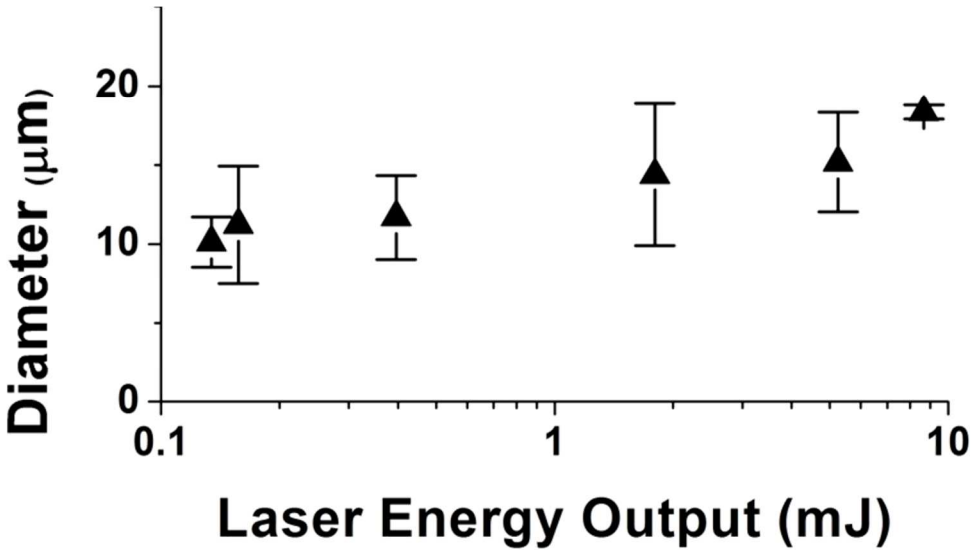

Figure S1. Spot diameters as a function of the mid-IR laser energy output measured on thermal paper.

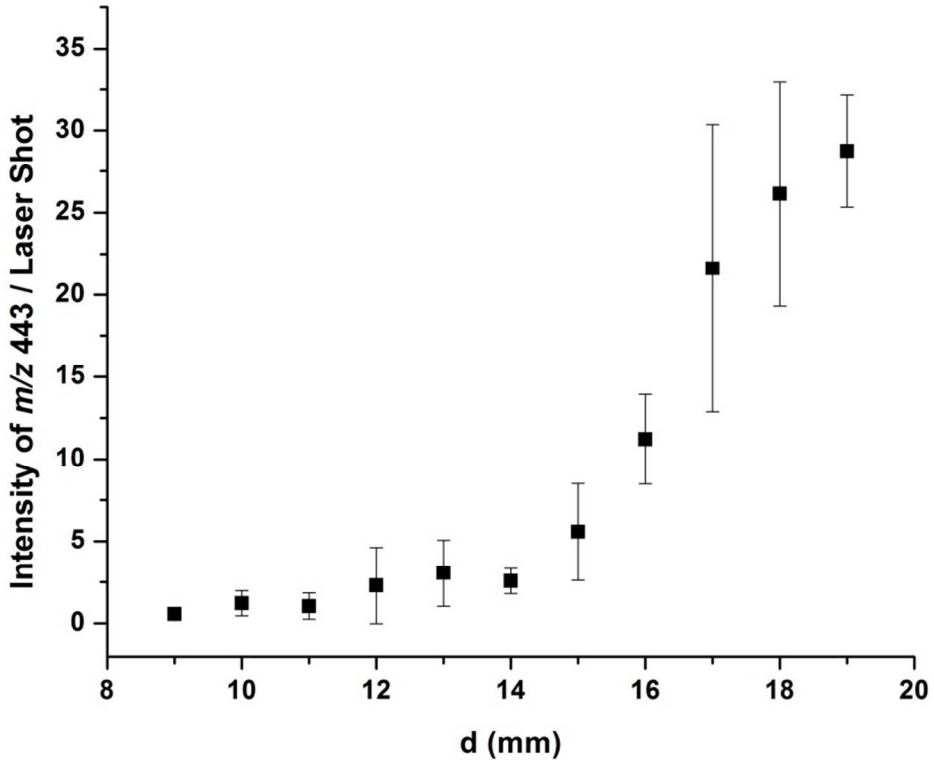

Figure S2. Above a threshold, signal intensity is highly dependent on the distance, d, between the sample, and the axis defined by the mass spectrometer inlet orifice and electrospray emitter.

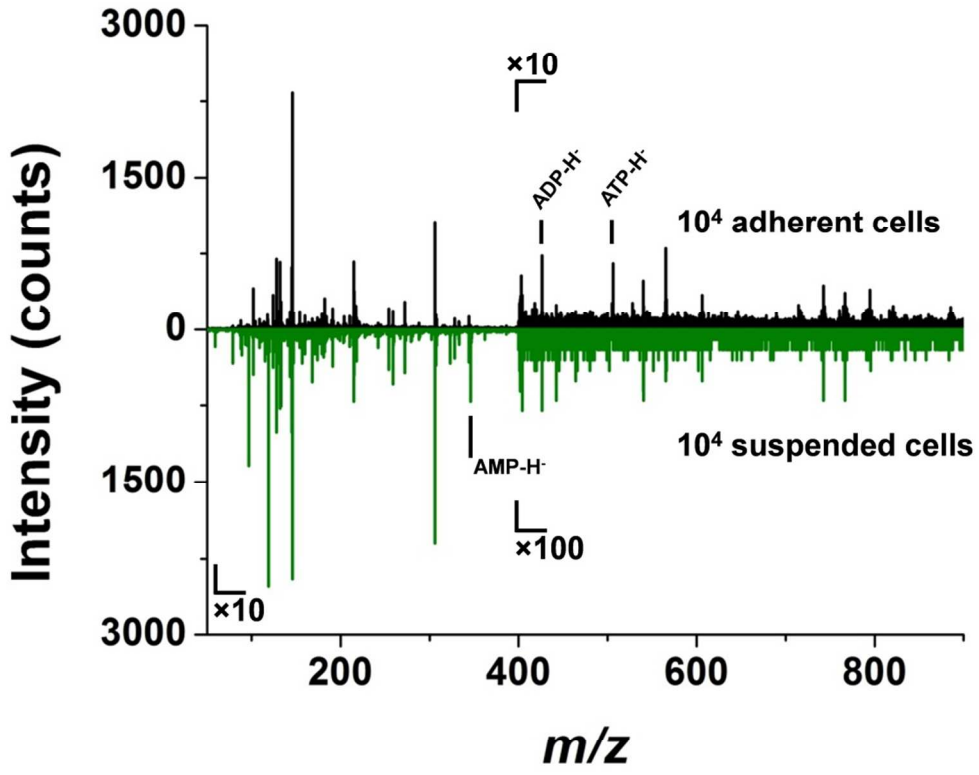

Figure S3. Comparison of spectra from ~10^4 adherent (top) and suspended (bottom) cells obtained using rg-LAESI-MS. Peaks in the adherent cell spectrum are ~10 times more abundant. The ATP peak intensity is marginal in the suspended cell spectrum, whereas the AMP peak is weak in the adherent cell spectrum.